NASA/TM-2009-214649

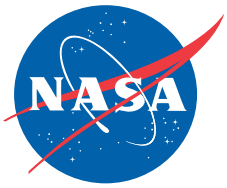

Static Aeroelastic Effects of Formation Flight for Slender Unswept Wings

Curtis E. Hanson
NASA Dryden Flight Research Center
Edwards, California

August 2009

NASA STI Program ... in Profile

Since its founding, NASA has been dedicated to the advancement of aeronautics and space science. The NASA scientific and technical information (STI) program plays a key part in helping NASA maintain this important role.

The NASA STI program operates under the auspices of the Agency Chief Information Officer. It collects, organizes, provides for archiving, and disseminates NASA's STI. The NASA STI program provides access to the NASA Aeronautics and Space Database and its public interface, the NASA Technical Report Server, thus providing one of the largest collections of aeronautical and space science STI in the world. Results are published in both non-NASA channels and by NASA in the NASA STI Report Series, which includes the following report types:

- TECHNICAL PUBLICATION. Reports of completed research or a major significant phase of research that present the results of NASA Programs and include extensive data or theoretical analysis. Includes compilations of significant scientific and technical data and information deemed to be of continuing reference value. NASA counterpart of peer-reviewed formal professional papers but has less stringent limitations on manuscript length and extent of graphic presentations.

- TECHNICAL MEMORANDUM. Scientific and technical findings that are preliminary or of specialized interest, e.g., quick release reports, working papers, and bibliographies that contain minimal annotation. Does not contain extensive analysis.

- CONTRACTOR REPORT. Scientific and technical findings by NASA-sponsored contractors and grantees.

- CONFERENCE PUBLICATION. Collected papers from scientific and technical conferences, symposia, seminars, or other meetings sponsored or co-sponsored by NASA.

- SPECIAL PUBLICATION. Scientific, technical, or historical information from NASA programs, projects, and missions, often concerned with subjects having substantial public interest.

- TECHNICAL TRANSLATION. English-language translations of foreign scientific and technical material pertinent to NASA's mission.

Specialized services also include creating custom thesauri, building customized databases, and organizing and publishing research results.

For more information about the NASA STI program, see the following:

- Access the NASA STI program home page at *http://www.sti.nasa.gov*

- E-mail your question via the Internet to help@sti.nasa.gov

- Fax your question to the NASA STI Help Desk at 443-757-5803

- Phone the NASA STI Help Desk at 443-757-5802

- Write to:
  NASA STI Help Desk
  NASA Center for AeroSpace Information
  7115 Standard Drive
  Hanover, MD 21076-1320

NASA/TM-2009-214649

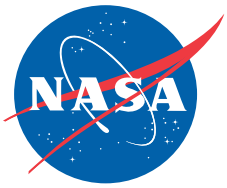

Static Aeroelastic Effects of Formation Flight for Slender Unswept Wings

Curtis E. Hanson
NASA Dryden Flight Research Center
Edwards, California

National Aeronautics and
Space Administration

Dryden Flight Research Center
Edwards, California 93523-0273

August 2009

NOTICE

Use of trade names or names of manufacturers in this document does not constitute an official endorsement of such products or manufacturers, either expressed or implied, by the National Aeronautics and Space Administration.

Available from:

NASA Center for AeroSpace Information
7115 Standard Drive
Hanover, MD 21076-1320
(443) 757-5802

ABSTRACT

The static aeroelastic equilibrium equations for slender, straight wings are modified to incorporate the effects of aerodynamically-coupled formation flight. A system of equations is developed by applying trim constraints and is solved for component lift distribution, trim angle-of-attack, and trim aileron deflection. The trim values are then used to calculate the elastic twist distribution of the wing box. This system of equations is applied to a formation of two gliders in trimmed flight. Structural and aerodynamic properties are assumed for the gliders, and solutions are calculated for flexible and rigid wings in solo and formation flight. It is shown that formation disturbances produce greater twist in the wingtip immersed in the vortex than for either the opposing wingtip or the wings of a similar airplane in solo flight. Changes in the lift distribution, resulting from wing twist, increase the performance benefits of formation flight. A flexible wing in formation flight will require greater aileron deflection to achieve roll trim than a rigid wing.

NOMENCLATURE

a	linear intercept
A	area, meters squared
AR	aspect ratio
b	wingspan, meters
c	chord length, meters
c_a	chord length of the aileron, meters
c_l	lift coefficient, non-dimensional
c_m	pitching moment coefficient, non-dimensional
c_{d_i}	induced drag coefficient, non-dimensional
c_{l_α}	sectional lift-curve slope, per radian
c_r	chord length at the wing root, meters
ccl	chord length times lift coefficient, meters
$\{cc_l\}$	span-wise vector of chord length times lift coefficient, meters
$\left\{cc_l^r\right\}_p^a$	span-wise vector of rigid-wing lift due to roll rate, meters per radian per second
$\{c_m\}$	span-wise vector of pitching moment coefficient, non-dimensional
$\{c_m\}_{\delta_a}$	span-wise vector of pitching moment coefficient due to aileron deflection, per radian
$\left[C^{\theta\theta}\right]$	torsional influence coefficient matrix, radians per kilogram per meter
d	distance from the wing center of gravity to the aerodynamic center, meters
e	distance from the wing elastic axis to the aerodynamic center, meters
$[E]$	integrated influence coefficient matrix times the elastic axis, meters per kilogram
$[F]$	integrated influence coefficient matrix times the chord squared, meters squared per kilogram
g	gravitational acceleration, meters per second squared
G	modulus of rigidity, kilograms per meter squared
$[G]$	integrated influence coefficient matrix times the center of gravity, meters per kilogram
J	torsional constant, meters to the fourth power
k	intermediate calculation

m	mass, kilograms
$\{m_w\}$	span-wise vector of wing mass, kilograms
n	Fourier sine series term
n_z	load factor, non-dimensional
p	roll rate, radians per second
$\dot{p}$	roll acceleration, radians per second squared
q	dynamic pressure, kilograms per meter per second squared
r_c	viscous core radius, meters
s	distance, meters
t	material thickness, meters
u	unperturbed dependent sensitivity parameter
$\tilde{u}$	perturbed dependent sensitivity parameter
v	unperturbed independent sensitivity parameter
V	airspeed, meters per second
$\tilde{v}$	perturbed independent sensitivity parameter
$\left[\bar{W}\right]$	integration weighting matrix, meters
y	span-wise coordinate, meters
$y(\Delta\lambda)$	span-wise location of change in taper ratio, meters
α	angle-of-attack, radians
α_0	angle-of-attack at zero lift coefficient, radians
$[A]$	aerodynamic operator, radians per meter
γ	maximum wingbox thickness in fraction of chord length
Γ_0	circulation strength, meters squared per second
δ_a	aileron deflection, radians
Δ	change in parameter
Δy	lateral separation between wing centerlines, meters
$\{\theta\}$	span-wise vector of wing twist angle, radians
λ	wing taper ratio
ρ	atmospheric density, kilograms per cubic meter
ϕ	wing station

Subscripts

FF	formation flight
i	inner wing section, from the wing root to the change in taper ratio
o	outer wing section, from the change in taper ratio to the wingtip
δ_a	aileron deflection

Superscripts

a	antisymmetrical
as	asymmetrical
e	elastic
ib	inboard semi-span, nearest to the leading wing
ob	outboard semi-span, furthest from the leading wing
r	rigid
s	symmetrical

INTRODUCTION

For two aircraft flying in formation, certain formation geometries will produce aerodynamic disturbances on one or both airplanes. Generally speaking, if the airplanes are co-planar in a wingtips-aligned echelon formation with 3-5 wingspans of longitudinal separation, the trailing airplane will experience a combination of lift force and roll moment due to the wingtip vortices of the leading plane. By re-trimming to account for these disturbances, the trailing airplane is typically able to achieve a reduction in drag of 10-20% (refs. 1-3).

Static aeroelastic deflections of the trailing wing in a formation have the potential to alter its lift distribution. For flexible wings, such aeroelastic effects may need to be considered when analyzing trim requirements or when making performance predictions.

The majority of published literature on aerodynamically-coupled formation flight deals with aerodynamic modeling, automatic control system design, and to a lesser extent, performance measurements from wind-tunnel and flight test experiments. Very little published work is available which addresses methods for calculating static aeroelastic effects for a wing in formation flight. Iglesias (ref. 4) gives a method for optimizing the span load of wings in formation flight, but does not include elastic deformations.

This paper presents a method for determining the static aeroelastic effects of formation flight disturbances on a slender, straight wing. Straight wings eliminate the need to consider the effects of wing bending on local angle-of-attack, leaving only the twisting of the wing to be accounted for in the aeroelastic theory. Furthermore, the effects of sweep need not be included in the aerodynamic theory. Sailplanes commonly employ slender, unswept wings and have been reported to use formation flight for drag reduction (refs. 5-7). Results are presented for an example sailplane.

FORMATION FLIGHT AERODYNAMICS

The relative geometry of two wings in an aerodynamically-coupled formation is shown in figure 1. The wings are assumed to be co-planar and of sufficient longitudinal separation that there are no formation-induced disturbances acting on the leading wing. A coordinate system is specified such that span-wise coordinates are referenced to the centerline of the trailing wing. The leading wing is modeled as a horseshoe vortex, which consists of a bound vortex along the wing, and semi-infinite trailing vortices streaming from the wingtips. The trailing wing is modeled using lifting-line theory.

The circulation, or strength per unit length, of the semi-infinite trailing vortices is assumed to be equal to that of the bound vortex along the wing. For longitudinal separations of three to five wingspans, viscous dissipation of the vortex strength can be neglected. The circulation is approximated with equation (1) by applying the Kutta-Joukowski theorem (ref. 8) for a wing in 1-*g* wings-level trimmed flight.

$$\Gamma_0 = \frac{mg}{\rho V \frac{\pi}{4} b} \tag{1}$$

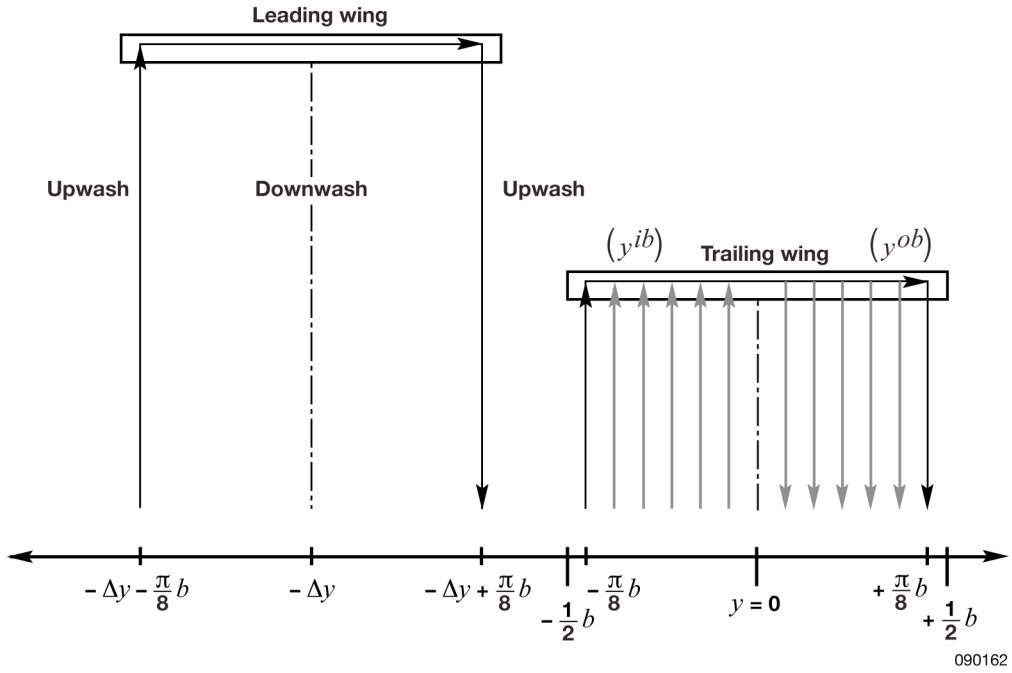

Figure 1. Formation geometry.

Following standard practice for horseshoe vortices, the circulation is held constant along the span and set equal to the circulation at the symmetry plane of a wing with an elliptical lift distribution. This assumption requires that the semi-infinite trailing vortices be separated by the effective span $\frac{\pi}{4}b$. While this model of the wing is not exact, it does capture the fact that maximum induced drag benefit is achieved with some wing overlap in the span-wise direction. This real life phenomenon is due to the rolling up of the wing tip vortices, which is not modeled in this paper.

For a known span-wise separation distance Δy between the wings, it is necessary to calculate the induced angle-of-attack at any point y along the trailing wing due to both trailing vortices of the lead wing. Applying the Burnham-Hallock tangential velocity profile for a vortex (ref. 9) and small-angle approximation, the induced angle-of-attack is shown in equation (2):

$$\alpha(y)_{FF} = \frac{\Gamma_0}{2\pi V}\left[\frac{\Delta y - \frac{\pi}{8}b + y}{\left(\Delta y - \frac{\pi}{8}b + y\right)^2 + r_c^2} - \frac{\Delta y + \frac{\pi}{8}b + y}{\left(\Delta y + \frac{\pi}{8}b + y\right)^2 + r_c^2}\right] \tag{2}$$

The use of a viscous vortex core eliminates singularities at the vortex center. The radius r_c of the viscous core can be chosen as 3% of the wingspan as recommended by Blake (ref. 10).

The vortex-induced angle-of-attack distributions across a trailing wing are shown in figure 2 for three different formation geometries. The maximum induced upwash across the trailing wing is achieved when its wingtip is exactly aligned with the nearest vortex core, corresponding to the point of minimum induced drag. Increasing the lateral separation between the wings causes the trailing wing to miss the region of largest upwash, while reducing separation causes the trailing wing to encounter a significant region of downwash. Note that, for all three lateral separations, the angle-of-attack distributions are asymmetric with respect to the centerline of the trailing wing.

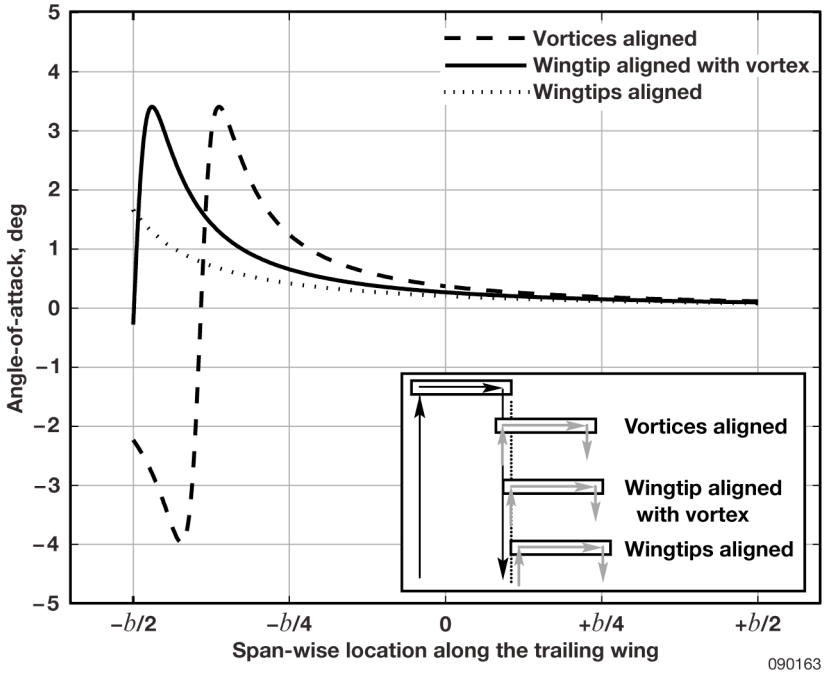

Figure 2. Vortex-induced angle-of-attack distribution.

STATIC AEROELASTIC EQUILIBRIUM EQUATIONS

The equations of static aeroelastic equilibrium are presented in the general matrix form used by Bisplinghoff (ref. 11), and are modified to include formation flight disturbances as well as to account for a wing in trimmed flight. The modified equilibrium equations are combined with additional trim constraint equations; and the resulting system is solved simultaneously for the wing lift distribution, trim rigid-wing angle-of-attack, and trim aileron deflection.

General Equations Including Formation Effects

Matrix forms of the symmetrical and antisymmetrical static aeroelastic equilibrium equations are given in equations (3a) and (3b) (ref. 11). These equations are augmented by adding the asymmetrical equation (3c) to account for formation flight effects:

$$\left[A^s\right]\{cc_l\}^s = q[E]\{cc_l\}^s + \left[A^s\right]\left\{cc_l^r\right\}^s + q[F]\{c_m\} - n_z[G]\{m_w g\} \tag{3a}$$

$$\left[A^a\right]\{cc_l\}^a = q[E]\{cc_l\}^a + \left[A^a\right]\left(\left\{cc_l^r\right\}_{\delta_a}^a \delta_a + \left\{cc_l^r\right\}_p^a p\right) + q[F]\{c_m\}_{\delta_a}\delta_a - [G][y]\{m_w\}\dot{p} \tag{3b}$$

$$\left[A^{as}\right]\{cc_l\}^{as} = q[E]\{cc_l\}^{as} + \left[A^{as}\right]\left\{cc_l^r\right\}_{FF}^{as} \tag{3c}$$

where

$$[E] = \left[C^{\theta\theta}\right][e]\left[\bar{W}\right],$$
$$[F] = \left[C^{\theta\theta}\right]\left[c^2\right]\left[\bar{W}\right], \text{ and}$$
$$[G] = \left[C^{\theta\theta}\right][d]\left[\bar{W}\right]$$

The left-hand side of equation (3) represents the symmetrical, antisymmetrical and asymmetrical angle-of-attack distributions across the trailing wing. The total angle-of-attack is composed of a rigid wing angle (the angle-of-attack that the free-stream would make with the un-deformed wing) and a deformed wing twist angle. The symmetrical equation includes the effects of the rigid-wing lift, the associated pitching moment about the aerodynamic center, and the weight of the wing itself. Antisymmetrical effects include lift force and pitching moment due to aileron deflection, lift due to roll, and an inertial force due to roll acceleration. The asymmetrical effects are simply due to the lift obtained from the upwash of the leading wing.

The aerodynamic operators $\left[A^s\right]$ and $\left[A^a\right]$ can be computed with Prandtl's lifting line theory using equation (4), which accounts for symmetrical and antisymmetrical effects. The asymmetrical operator $\left[A^{as}\right]$ must be calculated using a different theory, such as aerodynamic strip theory shown in equation (5), where the lift coefficient at each wing station is dependent only upon its local angle-of-attack.

$$[A] = \left[\frac{1}{a_0 c}\right] + \frac{1}{4b}\left[\frac{1}{\sin\phi}\right][n\sin n\phi][\sin n\phi]^{-1} \tag{4}$$

$$[A] = \left[\frac{1}{a_0 c}\right] \tag{5}$$

Equilibrium Equations for Trimmed Formation Flight

If both wings are in 1-*g* wings-level trimmed flight; the load factor, roll rate, and roll acceleration can be assumed as shown in equations (6a) and (6b):

$$n_z = 1 \tag{6a}$$

$$p = \dot{p} = 0 \tag{6b}$$

Also for trimmed flight, the symmetric aerodynamic operator can be used to express the rigid wing lift distribution in terms of the scalar rigid-wing angle-of-attack as shown in equation (7):

$$\left[A^s\right]\left\{cc_l^r\right\}^{\mathrm{s}} = \{1\}\alpha^r \tag{7}$$

The lift due to the formation flight term can similarly be expressed using the asymmetric aerodynamic operator as shown in equation (8):

$$\left[A^{as}\right]\left\{cc_l^r\right\}_{FF}^{as} = \{\alpha\}_{FF} \tag{8}$$

The resulting trimmed equations of equilibrium are shown in equations (9a), (9b), and (9c) respectively:

$$\left[A^s\right]\{cc_l\}^s = q[E]\{cc_l\}^s + \{1\}\alpha^r + q[F]\{c_m\} - [G]\{m_w g\} \tag{9a}$$

$$\left[A^a\right]\{cc_l\}^a = q[E]\{cc_l\}^a + \left(\left[A^a\right]\left\{cc_l^r\right\}_{\delta_a}^a + q[F]\{c_m\}_{\delta_a}\right)\delta a \tag{9b}$$

$$\left[A^{as}\right]\{cc_l\}^{as} = q[E]\{cc_l\}^{as} + \{\alpha\}_{FF} \tag{9c}$$

The trailing wing-half nearest to the leading wing's vortices will be referred to as the inboard (ib) wing, and the wing half farthest away will be referred to as the outboard (ob) wing. The six equations that result when equations (9a), (9b), and (9c) are applied separately to the inboard and outboard halves of the trailing wing contain 10 unknowns. Six of these are vector unknowns consisting of the symmetrical $\{cc_l\}^s$, antisymmetrical $\{cc_l\}^a$, and asymmetrical $\{cc_l\}^{as}$ lift distributions for both the inboard and outboard wing segments. The four remaining unknowns are the scalar values of trim angle-of-attack α^r and aileron deflection δ_a for each wing half.

Equations (10a) and (10b) are derived from the symmetric and antisymmetric relationships between the two wing halves and reduce the problem to four equations and eight unknowns:

$$\{cc_l\}^{s-ob} = \{cc_l\}^{s-ib} = \{cc_l\}^{s} \tag{10a}$$

$$\{cc_l\}^{a-ob} = -\{cc_l\}^{a-ib} = \{cc_l\}^{a} \tag{10b}$$

Two additional equations, (11a) and (11b), can be written to reduce the number of scalar unknowns from four to two. Note that the relationship in equation (11b) assumes that the deflection of the inboard and outboard ailerons is equal and opposite in direction.

$$\alpha^{r-ib} = \alpha^{r-ob} = \alpha^{r} \tag{11a}$$

$$\delta_a^{ib} = -\delta_a^{ob} = \delta_a \tag{11b}$$

The resulting system contains four equations and six unknowns. Clearly, two additional equations must be constructed in order to find a solution. These two equations result from the 1-*g* and wings-level trim constraints on the trailing wing. Under the assumption that the aircraft flight path angle is very near zero, 1-*g* trim is achieved when the component of the total lift force normal to the free-stream velocity is equal to the weight of the airplane. The symmetric lift terms, both rigid-wing and elastic-wing, are aligned according to the rigid-wing angle-of-attack and are therefore normal to the free stream. However, the asymmetric terms are rotated slightly forward due to the vortex-induced upwash and must be resolved into components relative to the free stream. Note that, a component of the associated asymmetric induced drag will contribute to the total aircraft lift. However, this contribution is assumed to be negligible and is not accounted for. Recognizing that the antisymmetrical lift cancels and the symmetrical lift is equal between the two wing halves, the resulting 1-*g* trim equation is shown as equation 12:

$$q\lfloor 2 \rfloor [\bar{W}]\{cc_l\}^{s} + q\lfloor 1 \rfloor [\bar{W}]\left[\cos\{\alpha\}_{FF}^{ib}\right]\{cc_l\}^{as-ib} + q\lfloor 1 \rfloor [\bar{W}]\left[\cos\{\alpha\}_{FF}^{ob}\right]\{cc_l\}^{as-ob} = mg \tag{12}$$

Wings-level trim is achieved when the rolling moment between the two wing halves is of equal magnitude and opposite sign. As in the 1-*g* trim case, the asymmetric lift terms are resolved into their components perpendicular to the free stream. The symmetric moment terms cancel and the antisymmetric terms sum together as shown in equation (13):

$$2\left\lfloor y^{ob}\right\rfloor\left[\bar{W}\right]\left\{cc_l\right\}^{a}+\left\lfloor y^{ib}\right\rfloor\left[\bar{W}\right]\left[\cos\left\{\alpha\right\}_{FF}^{ib}\right]\left\{cc_l\right\}^{as-ib}+\left\lfloor y^{ob}\right\rfloor\left[\bar{W}\right]\left[\cos\left\{\alpha\right\}_{FF}^{ob}\right]\left\{cc_l\right\}^{as-ob}=0 \tag{13}$$

The system of six equations and six unknowns can now be solved using matrix inversion. The solution can be written as shown in equation (14):

$$\begin{bmatrix}\left\{cc_l\right\}^{s}\\ \left\{cc_l\right\}^{a}\\ \left\{cc_l\right\}^{as-ib}\\ \left\{cc_l\right\}^{as-ob}\\ \alpha^{r}\\ \delta_a\end{bmatrix}=[Q]^{-1}[R]$$

where

$$[Q]=\begin{bmatrix}\left[A^{s}\right]-q[E] & [0] & [0] & [0] & -\{1\} & \{0\}\\ [0] & \left[A^{a}\right]-q[E] & [0] & [0] & \{0\} & \left[A^{a}\right]\left\{cc_l^{r}\right\}_{\delta_a}^{a}+q[F]\{c_m\}_{\delta_a}\\ [0] & [0] & \left[A^{as}\right]-q[E] & [0] & \{0\} & \{0\}\\ [0] & [0] & [0] & \left[A^{as}\right]-q[E] & \{0\} & \{0\}\\ q\lfloor 2\rfloor\left[\bar{W}\right] & \lfloor 0\rfloor & q\lfloor 1\rfloor\left[\bar{W}\right]\left[\cos\left\{\alpha\right\}_{FF}^{ib}\right] & q\lfloor 1\rfloor\left[\bar{W}\right]\left[\cos\left\{\alpha\right\}_{FF}^{ob}\right] & 0 & 0\\ \lfloor 0\rfloor & 2\left\lfloor y^{ob}\right\rfloor\left[\bar{W}\right] & \left\lfloor y^{ib}\right\rfloor\left[\bar{W}\right]\left[\cos\left\{\alpha\right\}_{FF}^{ib}\right] & \left\lfloor y^{ob}\right\rfloor\left[\bar{W}\right]\left[\cos\left\{\alpha\right\}_{FF}^{ob}\right] & 0 & 0\end{bmatrix}$$

$$[R]=\begin{bmatrix}q[F]\{c_m\}-[G]\left\{\frac{1}{2}m_w g\right\}\\ \{0\}\\ \{\alpha\}_{FF}^{ib}\\ \{\alpha\}_{FF}^{ob}\\ mg\\ 0\end{bmatrix} \tag{14}$$

Wing Twist Calculations

Once the solution to equation (14) is found, the wing torsional deflections can be computed. The total lift of the wing is divided into a rigid wing term and an elastic wing term as shown in equation (15):

$$\{cc_l\} = \left\{cc_l^r\right\} + \left\{cc_l^e\right\} \tag{15}$$

The twist angle is related to the elastic wing lift term through the appropriate aerodynamic operator as shown in equation (16):

$$\{\theta\} = [A]\left\{cc_l^e\right\} \tag{16}$$

By substituting the appropriate forms of equations (15) and (16) into the symmetrical, antisymmetrical, and asymmetrical trimmed equilibrium equations (9a), (9b), and (9c); equations (17a), (17b), and (17c) are developed to calculate the wing twist equations for a given wing segment:

$$\{\theta\}^s = \left[A^s\right]\left(\left[A^s\right] - q[E]\right)^{-1}\left(q[E]\left[A^s\right]^{-1}\{1\}\alpha^r + q[F]\{c_m\} - [G]\left\{\tfrac{1}{2}m_w g\right\}\right) \tag{17a}$$

$$\{\theta\}^a = \left[A^a\right]\left(\left[A^a\right] - q[E]\right)^{-1}\left(q[E]\left\{cc_l^r\right\}_{\delta_a}^{a}\ \delta_a + q[F]\{c_m\}_{\delta_a}\ \delta_a\right) \tag{17b}$$

$$\{\theta\}^{as} = \left[A^{as}\right]\left(\left[A^{as}\right] - q[E]\right)^{-1}\left(q[E]\left[A^{as}\right]^{-1}\{\alpha\}_{FF}\right) \tag{17c}$$

See Appendix A for a detailed derivation of equations (17a), (17b), and (17c).

Rigid–Wing and Solo–Flight Solutions

For the purposes of comparison, it is desirable to obtain solutions for the same wing in solo flight as well as a similar but rigid wing in formation flight. For a flexible wing in solo flight, the vortex-induced angle-of-attack is set to zero in equation (2). Equations (14) and (17) are then solved as before. The solution for a rigid wing in formation flight is determined by setting the influence coefficient matrix in equations (3a), (3b), and (3c) to all zeros, effectively zeroing out the matrices $[E]$, $[F]$, and $[G]$. Equation (14) is then solved as before.

Performance Calculations

An assessment of the impact of wing twist on the performance benefits of formation flight requires an examination of the induced drag of the trailing wing. Additional flexible wing effects on aircraft performance such as profile drag due to wing twist and increased aileron deflection are not addressed here, but may be significant.

The induced drag for a wing is typically a function of the square of the lift coefficient. For a wing in formation flight, there is an additional term due to the rotation of the lift vector resulting from the vortex-induced angle-of-attack. The induced drag coefficient at a given wing section is calculated as shown in equation 18:

$$c_{d_i} = \frac{\left(c_l^s + c_l^a + c_l^{as}\cos\alpha_{FF}\right)^2}{\pi AR} - c_l^{as}\sin\alpha_{FF} \tag{18}$$

SAILPLANE EXAMPLE

As an example, rigid wing and flexible wing trim and performance calculations will be carried out for a formation of two sailplanes, which are similar to the Nimbus II (Schempp-Hirth Flugzeugbau GmbH, Kirchheim unter Teck, Germany) open-class fiberglass sailplane designed in 1971 by Klaus Holighaus (ref. 12). Airfoil, performance, and geometric data for the example sailplane are listed in table 1. The formation is analyzed at the airspeed for best lift-to-drag ratio given in table 1 and at an altitude of 5,000 ft. The following plane's left inboard wingtip is assumed to be aligned with the leading plane's right wingtip vortex. This is the location of maximum drag reduction, as described earlier in the Formation Flight Aerodynamics section.

Other than for mass considerations when calculating trim lift, each airplane is treated as a single wing with no fuselage or empennage. Each wing half of the trailing plane is divided into 300 stations, and an integration-weighting matrix is calculated according to the Multhopp quadrature formula (ref. 11). All integrations are performed from the wingtip toward the wing root.

Table 1. Example sailplane characteristics (ref. 12).

Characteristic	Value
General	
Mass:	500 kg
Best glide airspeed:	105 km per hr
Max lift-to-drag ratio:	47.5
Wing	
Airfoil (FX 67-K-170):	
Maximum thickness	0.17 *c*
Span:	20.3 m
Area:	14.41 m^2
Chord:	
Root	0.96 m
Taper ratio, inner	0.75
Taper ratio, outer	0.36
Taper change point	0.57 *b*
Twist:	0^o
Wing mass:	230 kg
Aileron	
Span:	
Inboard edge	0.57 *b*
Outboard edge	0.95 *b*
Chord:	0.12 m

Structural Model

A simple model of the sailplane wing was constructed by assuming certain structural properties. Bending of the wing was neglected since only the torsional influence function appears in the aeroelastic equilibrium equations. A rectangular single-cell wing box was assumed as shown in figure 3.

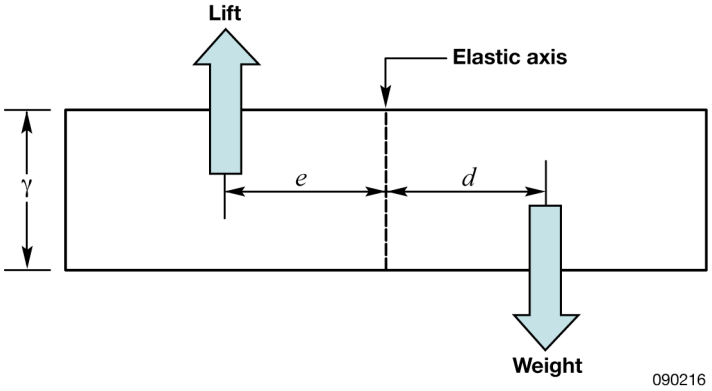

Figure 3. Single-cell wing box.

The torsional influence function can then be computed for each wing using equation (19):

$$C^{\theta\theta} = \frac{1}{2kk_i}\left[\frac{1}{(1-k_i y)^2} - 1\right] \quad , \qquad 0 \le y \le y(\Delta\lambda)$$

$$C^{\theta\theta} = C^{\theta\theta}\left(y(\Delta\lambda)\right) + \frac{1}{2kk_o^2}\left[\frac{1}{\left(k_o^1 - k_o^2 y\right)^2} - \frac{1}{\left(k_o^1 - k_o^2 y(\Delta\lambda)\right)^2}\right] \quad , \qquad y(\Delta\lambda) \le y \le \tfrac{1}{2}b$$

where

$$k = \frac{tG\gamma^2 c_r^3}{2\gamma^2 + 1}$$

$$k_i = \frac{1-\lambda_i}{y(\Delta\lambda)}$$

$$k_o^1 = \frac{\frac{1}{2}b\lambda_i - \lambda_o y(\Delta\lambda)}{\frac{1}{2}b - y(\Delta\lambda)}$$

$$k_o^2 = \frac{\lambda_i - \lambda_o}{\frac{1}{2}b - y(\Delta\lambda)} \tag{19}$$

A detailed derivation of equation (19) is contained in Appendix B.

Constant values for the modulus of rigidity and structural wall thickness were obtained for eight plies of E-Glass 7781 fiberglass (ref. 13) as $G = 758 \times 10^3$ pounds per square inch and $t = 0.0085$ inches per ply, respectively. Values for the location of the elastic axis relative to the quarter-chord line (e) and to the chord-wise center of gravity (d) are given in table 2 along with the wing box height (γ). As a first-order approximation, the distribution of wing mass along the semi-span was assumed to be proportional to the volume of the wing box.

Table 2. Wing box parameters.

Parameter	Value
e	0.1250 c
d	–0.1250 c
γ	0.1275 c

Aerodynamic Model

Values for the necessary wing aerodynamic parameters and coefficients are summarized in table 3. The angle-of-attack for zero lift and pitching moment coefficient for the FX 67-K-170 airfoil were taken from data published by Hansman and Craig (ref. 14). The sectional lift-curve slope was approximated as shown in equation (20):

$$c_{l_\alpha} = 2\pi \frac{AR}{AR+2} \tag{20}$$

Table 3. Wing aerodynamic properties.

Property	Value
c_{l_α}	5.8725 per radian
α_0	-6.33 deg
c_m	-0.102
$c_{l_{\delta_a}}$	1.25 to 1.69 per radian
$c_{m_{\delta_a}}$	-0.47 to -0.49 per radian

As recommended by Fung (ref. 15), the values for aileron lift and pitching moment coefficients were calculated as 80% of the theoretical values found using Glauret's approximations in equations (21) and (22), which are based upon the ratio of the aileron chord to the wing chord. The range of values in table 3 for these two parameters reflects the fact that the wing chord changes along the span.

$$c_{l_{\delta_a}} = 0.8 * \frac{c_{l_\alpha}}{\pi}\left[\cos^{-1}\left(1 - 2 * \frac{c_a}{c}\right) + 2\sqrt{\frac{c_a}{c}\left(1 - \frac{c_a}{c}\right)}\right] \tag{21}$$

$$c_{m_{\delta_a}} = -0.8 * \frac{c_{l_\alpha}}{\pi}\left[\left(1 - \frac{c_a}{c}\right)\sqrt{\frac{c_a}{c}\left(1 - \frac{c_a}{c}\right)}\right] \tag{22}$$

Results

The symmetrical, antisymmetrical, asymmetrical, and the combined total lift distributions across the trailing wing are shown in figure 4. The resulting lift distribution is significantly different from an elliptical distribution due to the combined effects of the nearby vortex and the aileron trim.

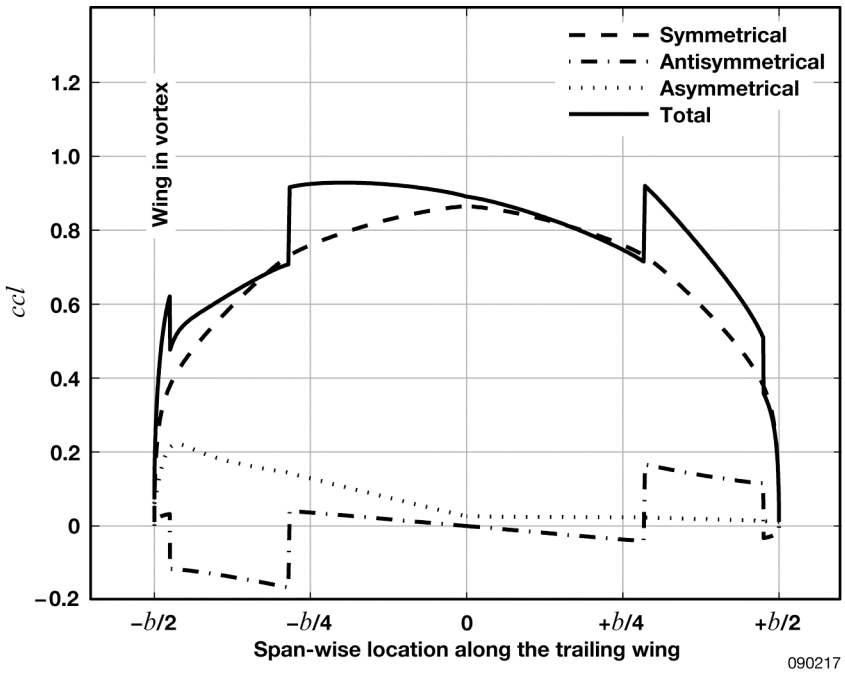

Figure 4. Lift distribution for a wing in formation flight.

Figure 5 shows a comparison of lift distributions between a flexible wing and a perfectly rigid wing, both in formation flight. The twisting of the flexible wing tends to reduce the lift at the root and increase it at the outer sections of the wing, where the ailerons are located, and for the inboard wing, where the vortex effects are strongest.

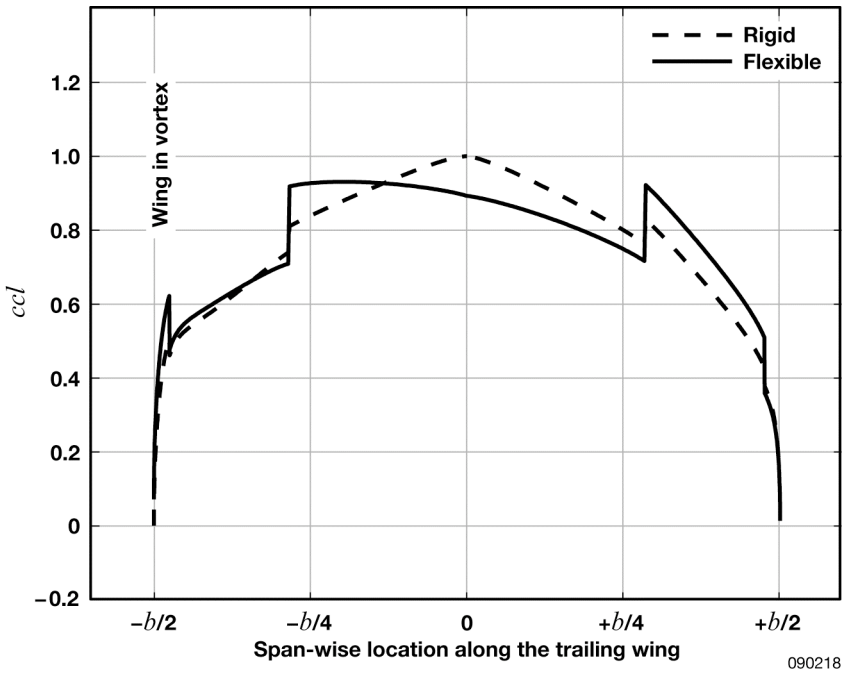

Figure 5. Comparison of lift distribution for flexible and rigid wings in formation flight.

The component and combined total wing twist distributions for the trailing wing are shown in figure 6. The twist of the inboard wingtip is significantly greater than that of the outboard tip. The lift force generated by the vortex upwash tends to twist the inboard wingtip in a positive sense, or leading edge up. The trailing edge up deflection of the aileron on the inboard wing also produces a positive twist. Conversely, vortex upwash effects on the outboard wing are negligible, and the trailing edge down aileron deflection produces a negative twist on that wing half.

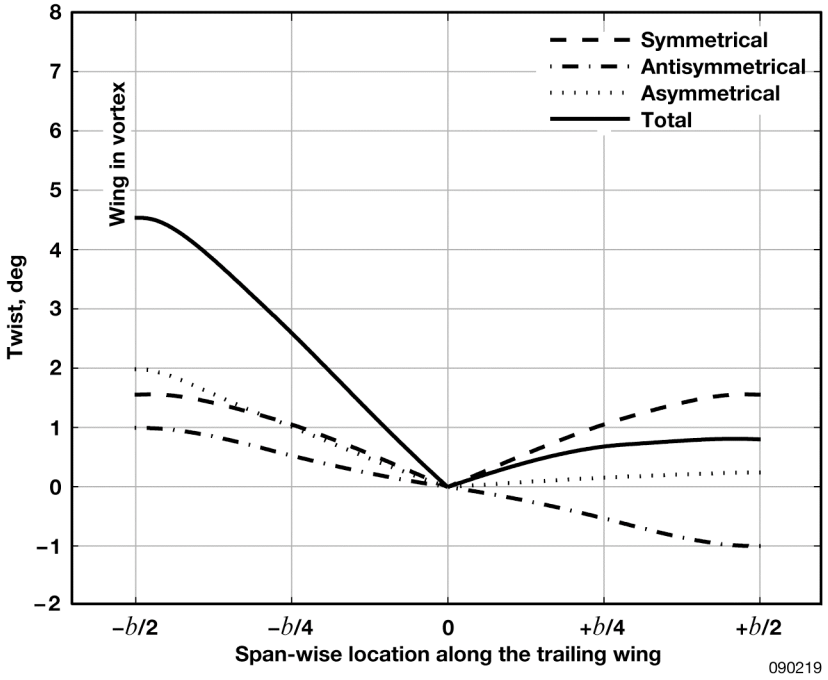

Figure 6. Wing twist distribution for a wing in formation flight.

Figure 7 shows a comparison of flexible wing twist between a wing flying in formation and a wing in solo flight. The wing in formation flight clearly exhibits greater twist on its inboard wing and reduced twist on its outboard wing. The solo wing experiences only symmetrical lift forces; therefore its twist distribution is symmetrical.

A comparison of induced drag for rigid and flexible wings in both solo and formation flight is shown in table 4. In solo flight, the induced drag is slightly higher for the flexible wing than for the rigid wing. This small drag penalty is a result of the energy required to maintain the twist of the wing.

Table 4. Induced drag.

	Rigid	Flexible
Solo flight	59.6 N	59.8 N
Formation flight	54.6 N	51.0 N

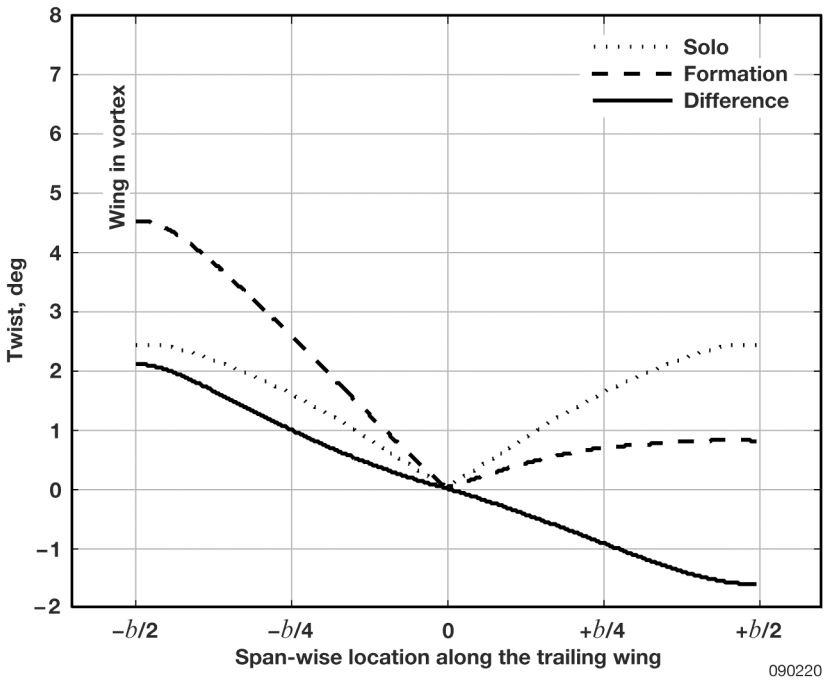

Figure 7. Comparison of wing twist for wings in formation flight and solo flight.

Formation flight yields an 8% reduction in induced drag for the rigid wing as compared to a 15% reduction for the flexible wing. This large discrepancy is attributable to the superposition of the inboard wing twist with the vortex-induced upwash distribution. The vortex-induced upwash causes the local lift vector to rotate forward creating a component that is parallel to the free-stream and acts in a negative drag sense. This effect is the source of drag reduction during formation flight. In the case of a flexible wing, the twisting of the wing redistributes the lift away from the wing root toward the wing tips. Therefore, the forward-rotated lift vector near the tip is of a larger magnitude for the flexible wing than for the rigid wing as is the associated negative drag component. Interestingly, the deflection of the inboard wing's aileron for roll trim has the opposite effect, reducing the lift near the tip along with the associated drag benefits. An alternate trim solution might alleviate this.

The trim aileron deflections for flexible and rigid wings in formation flight are shown in figure 8. The flexible wing requires significantly greater aileron deflection to trim out the vortex-induced rolling moment. Reduced torsional rigidity tends to reduce aileron effectiveness. Deflection of the aileron to increase lift produces a downward twist of the wing leading edge, reducing the lift generated by the wing. The increased aileron trim deflection for a flexible wing has the undesirable effect of increasing profile drag on the wing, which reduces the performance benefits gained through formation flight. As an example, experimental results for a high lift-to-drag ratio airfoil (ref. 16) indicate a profile drag coefficient increase of about 0.00006 per degree of flap deflection. Table 5 shows aircraft total drag for rigid and flexible wings in solo flight compared to total drag in formation flight with and without aileron trim drag effects. Aileron trim increases the total drag by about 0.2% in the case of the rigid wing, and by about 0.5% in the case of the flexible wing.

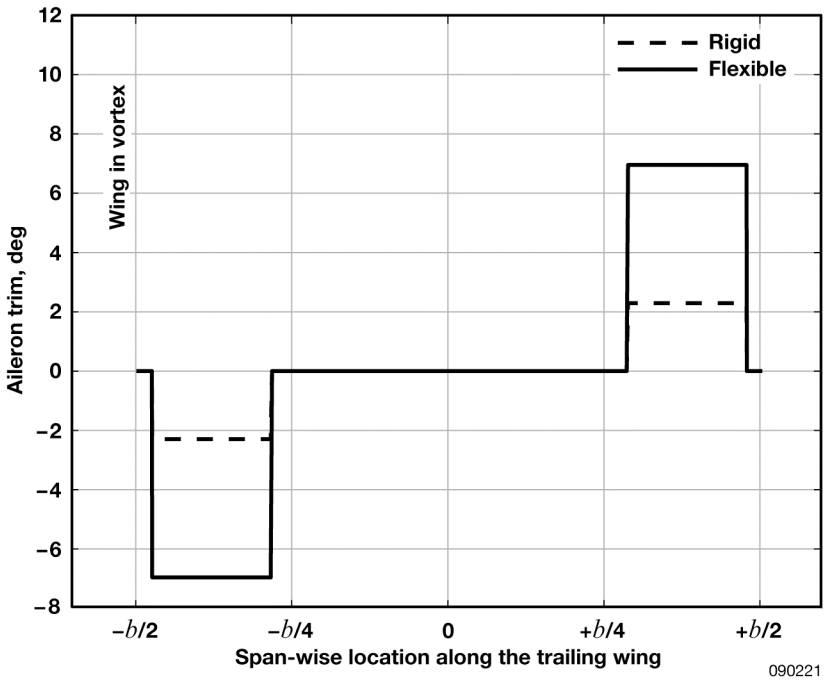

Figure 8. Comparison of aileron trim for flexible and rigid wings in formation flight.

Table 5. Total drag.

	Rigid	Flexible
Solo flight	103.2	103.4
Formation flight	98.2	94.6
Formation flight with aileron trim drag	98.4	95.1

The scaled sensitivities of induced drag and trim aileron deflection to various aircraft parameters can be calculated using equation (23). Perturbed values of flexible wing induced drag coefficient ($\tilde{c}_{d_i}$) and aileron trim deflection ($\tilde{\delta}_a$) were calculated for 1% changes in the wing structural and aerodynamic parameters listed in table 6.

$$\Delta u|_{\Delta v} = \frac{\tilde{u} - u}{\tilde{v} - v} \cdot \frac{v}{u} \tag{23}$$

Table 6. Sensitivity to estimated parameters.

$v =$	$u =$	
	c_{d_i}	δ_a
$G*t$	0.13	-1.9
e	-0.13	0.27
d	1.9e-4	-3.2e-4
c_m	-0.03	-3.2e-4
a_0	-0.30	1.9
$c_{l_{\delta_a}}$	-0.03	-2.7
$c_{m_{\delta_a}}$	0.03	1.8

The coefficient of induced drag is most strongly influenced by changes in the lift curve slope a_0, the wing torsional rigidity $G*t$, and the location of the wing elastic axis e. For example, a 1% increase in a_0 will reduce c_{d_i} by about 0.3%. A larger lift-curve slope results in a stronger lift vector rotated through the vortex-induced angle-of-attack. Increased torsional rigidity, and reduced spacing between the elastic axis and the quarter-chord line have the effect of resisting wing twist, which weakens the rotated lift vector and the associated reduction in induced drag.

As to be expected, roll-axis trim requirements are strongly affected by the aileron lift and moment coefficients. The required aileron trim deflection is also strongly influenced by the wing torsional rigidity and the lift-curve slope. The wing chord-wise center of gravity and pitching moment coefficient have little effect on either performance benefits or lateral trim requirements.

CONCLUSIONS

The static aeroelastic equilibrium equations for slender, straight wings were modified to incorporate the effects of aerodynamically-coupled formation flight. A system of equations was developed by applying trim constraints and was solved for component lift distribution, trim angle-of-attack, and trim aileron deflection. The trim values were then used to calculate the twist distribution of the wing. The system of equations was applied to a formation of two gliders in trimmed flight. Structural and aerodynamic properties were assumed for the gliders, and the solution was calculated for flexible and rigid wings in solo and formation flight.

In general, the inboard tip of a flexible wing in formation flight will tend to deflect a greater amount than the opposing wingtip. The inboard tip will also deflect a greater amount than the symmetrical deflection of a flexible wing in solo flight, while the outboard wingtip will deflect less. The outboard shift in lift distribution for a flexible wing has the effect of enhancing the performance benefits of formation flight. However, a flexible wing in formation flight will also tend to require greater roll trim input than a rigid wing, potentially resulting in slightly increased profile drag.

REFERENCES

1. Beukenberg, Markus, and Dietrich Hummel, "Aerodynamics, Performance and Control of Airplanes in Formation Flight," *Proceedings of the 17th Congress of the International Council of the Aeronautical Sciences,* ICAS-90-5.9.3, September 9-14 1990, pp. 1777-1794.

2. Vachon, M. Jake, Ronald J. Ray, Kevin R. Walsh, and Kimberly Ennix, "F/A-18 Aircraft Performance Benefits Measured During the Autonomous Formation Flight Project," AIAA 2002-4491, *Proceedings of the AIAA Flight Mechanics Conference and Exhibit*, August 5-8, 2002.

3. Wagner, Maj. Geno, Lt. Col. Dave Jacques, William Blake, and Meir Pachter, "Flight Test Results of Close Formation Flight for Fuel Savings," AIAA 2002-4490, *Proceedings of the AIAA Flight Mechanics Conference and Exhibit*, August 5-8, 2002.

4. Iglesias, Sergio, "Optimum Spanloads Incorporating Wing Structural Considerations And Formation Flying;" master's thesis, Virginia Polytechnic Institute and State University, November 10, 2000.

5. Reichmann, Helmut, *Cross-Country Soaring*, 7th ed., Soaring Society of America, Inc., Stuttgart, Germany, 2005.

6. Hummel, D., "The Use of Aircraft Wakes to Achieve Power Reductions in Formation Flight," *Proceedings of the 1996 AGARD FDP Symposium on The Characterisation & Modification of Wakes from Lifting Vehicles in Fluid*, AGARD CP-584, Paper No. 36, Trondheim, Norway, May 20-23, 1996, pp. 1-13.

7. Bramesfeld, Götz, "A Higher Order Vortex-Lattice Method with a Force-Free Wake;" Ph. D. Thesis, The Pennsylvania State University, August 2006.

8. Anderson, John D., Jr., *Fundamentals of Aerodynamics*, 2nd ed., McGraw-Hill, New York, 1991.

9. Burnham, D. C., and Hallock, J. N., "Chicago Monostatic Acoustic Vortex Sensing System, Volume IV: Wake Vortex Decay," DOT/FAA/RD-79-103, Vol. IV, July 1982, pp. 2-3.

10. Blake, William, and Dieter Multhopp, "Design, Performance and Modeling Considerations for Close Formation Flight," AIAA 98-4343, 1998.

11. Bisplinghoff, Raymond L., Holt Ashley, and Robert L. Halfman, *Aeroelasticity*, Dover Publications, Inc., New York, 1996.

12. Thomas, Fred, *Fundamentals of Sailplane Design*, College Park Press, College Park, Maryland, 1999.

13. *Composite Materials Handbook*, Vol. 2, Ch. 6, MIL-HDBK-17-2F, Department of Defense, June 17, 2002, pp. 44.

14. Hansman, R. John Jr., and Anthony P. Craig, "Low Reynolds Number Tests of NACA 64-210, NACA 0012 and Wortmann FX67-K170 Airfoils in Rain," *AIAA Journal of Aircraft*, Vol. 24, No. 8, August 1987, pp 559-566.

15. Fung, Y. C., *An Introduction to the Theory of Aeroelasticity*, John Wiley & Sons, Inc., New York, 1955, pp. 114-115.

16. Viken, Jeffrey K., Werner Pfenninger, and Robert J. McGhee, "Advanced Natural Laminar Flow Airfoil with High Lift to Drag Ratio," *Langley Symposium on Aerodynamics*, Vol. 1, December 1986, pp. 401-414.

APPENDIX A
DERIVATION OF EQUATIONS (17a), (17b) AND (17c)

Begin with equations (A1a) and (A1b), based upon equations (8-83) and (8-116), respectively from Bisplinghoff (ref. 11). Equation (A1c) follows the general form of equation (A1a), with the only asymmetric effect being the vortex-induced lift.

$$\left[A^s\right]\{cc_l\}^s = q[E]\{cc_l\}^s + \left[A^s\right]\left\{cc_l^r\right\}^s + q[F]\{c_m\} - n_z[G]\{m_w g\} \tag{A1a}$$

$$\left[A^a\right]\{cc_l\}^a = q[E]\{cc_l\}^a + \left[A^a\right]\left(\left\{cc_l^r\right\}_{\delta_a}^a \delta_a + \left\{cc_l^r\right\}_p^a p\right) + q[F]\{c_m\}_{\delta_a}\delta_a - [G][y]\{m_w\}\dot{p} \tag{A1b}$$

$$\left[A^{as}\right]\{cc_l\}^{as} = q[E]\{cc_l\}^{as} + \left[A^{as}\right]\left\{cc_l^r\right\}_{FF}^{as} \tag{A1c}$$

The simplifications listed in equations (6a) and (6b) are applied along with the definitions of the aerodynamic operators in equations (7) and (8). The three equations can then be written as equations (A2a), (A2b), and (A2c), which correspond to equations (9a), (9b), and (9c):

$$\left[A^s\right]\{cc_l\}^s = q[E]\{cc_l\}^s + \{1\}\alpha^r + q[F]\{c_m\} - [G]\{m_w g\} \tag{A2a}$$

$$\left[A^a\right]\{cc_l\}^a = q[E]\{cc_l\}^a + \left(\left[A^a\right]\left\{cc_l^r\right\}_{\delta_a}^a + q[F]\{c_m\}_{\delta_a}\right)\delta_a \tag{A2b}$$

$$\left[A^{as}\right]\{cc_l\}^{as} = q[E]\{cc_l\}^{as} + \{\alpha\}_{FF} \tag{A2c}$$

Bring some terms from the left-hand side to the right-hand side:

$$\left[A^s\right]\{cc_l\}^s - q[E]\{cc_l\}^s - \{1\}\alpha^r = q[F]\{c_m\} - [G]\{m_w g\} \tag{A3a}$$

$$\left[A^{a}\right]\{cc_l\}^{a} - q[E]\{cc_l\}^{a} = \left(\left[A^{a}\right]\left\{cc_l^{r}\right\}_{\delta_a}^{a} + q[F]\{c_m\}_{\delta_a}\right)\delta_a \tag{A3b}$$

$$\left[A^{as}\right]\{cc_l\}^{as} - q[E]\{cc_l\}^{as} = \{\alpha\}_{FF} \tag{A3c}$$

Factor out the $\{cc_l\}$ terms:

$$\left(\left[A^{s}\right] - q[E]\right)\{cc_l\}^{s} - \{1\}\alpha^{r} = q[F]\{c_m\} - [G]\{m_w g\} \tag{A4a}$$

$$\left(\left[A^{a}\right] - q[E]\right)\{cc_l\}^{a} = \left(\left[A^{a}\right]\left\{cc_l^{r}\right\}_{\delta_a}^{a} + q[F]\{c_m\}_{\delta_a}\right)\delta_a \tag{A4b}$$

$$\left(\left[A^{as}\right] - q[E]\right)\{cc_l\}^{as} = \{\alpha\}_{FF} \tag{A4c}$$

Now expand the $\{cc_l\}$ terms using equation (15):

$$\left(\left[A^{s}\right] - q[E]\right)\left\{cc_l^{e}\right\}^{s} + \left(\left[A^{s}\right] - q[E]\right)\left\{cc_l^{r}\right\}^{s} - \{1\}\alpha^{r} = q[F]\{c_m\} - [G]\{m_w g\} \tag{A5a}$$

$$\left(\left[A^{a}\right] - q[E]\right)\left\{cc_l^{e}\right\}^{a} + \left(\left[A^{a}\right] - q[E]\right)\left\{cc_l^{r}\right\}^{a} = \left(\left[A^{a}\right]\left\{cc_l^{r}\right\}_{\delta_a}^{a} + q[F]\{c_m\}_{\delta_a}\right)\delta_a \tag{A5b}$$

$$\left(\left[A^{as}\right] - q[E]\right)\left\{cc_l^{e}\right\}^{as} + \left(\left[A^{as}\right] - q[E]\right)\left\{cc_l^{r}\right\}^{as} = \{\alpha\}_{FF} \tag{A5c}$$

Isolate the elastic lift coefficient distribution vectors on the left-hand side:

$$\left\{cc_l^e\right\}^s = \left(\left[A^s\right] - q[E]\right)^{-1}\left(\left(-\left[A^s\right] + q[E]\right)\left\{cc_l^r\right\}^s + \{1\}\alpha^r + q[F]\{c_m\} - [G]\{m_w g\}\right) \tag{A6a}$$

$$\left\{cc_l^e\right\}^a = \left(\left[A^a\right] - q[E]\right)^{-1}\left(\left(-\left[A^a\right] + q[E]\right)\left\{cc_l^r\right\}^a + \left(\left[A^a\right]\left\{cc_l^r\right\}_{\delta_a}^a + q[F]\{c_m\}_{\delta_a}\right)\delta_a\right) \tag{A6b}$$

$$\left\{cc_l^e\right\}^{as} = \left(\left[A^{as}\right] - q[E]\right)^{-1}\left(\left(-\left[A^{as}\right] + q[E]\right)\left\{cc_l^r\right\}^{as} + \{\alpha\}_{FF}\right) \tag{A6c}$$

Now apply the following simplifying relations:

$$\left[A^s\right]\left\{cc_l^r\right\}^s = \{1\}\alpha^r \text{ and } \left\{cc_l^r\right\}^s = \left[A^s\right]^{-1}\{1\}\alpha^r \tag{A7a}$$

$$\left[A^a\right]\left\{cc_l^r\right\}^a = \left[A^a\right]\left\{cc_l^r\right\}_{\delta_a}^a\ \delta_a \text{ and } \left\{cc_l^r\right\}^a = \left\{cc_l^r\right\}_{\delta_a}^a\ \delta_a \tag{A7b}$$

$$\left[A^{as}\right]\left\{cc_l^r\right\}^{as} = \{\alpha\}_{FF} \text{ and } \left\{cc_l^r\right\}^{as} = \left[A^{as}\right]^{-1}\{\alpha\}_{FF} \tag{A7c}$$

Equations (A6a), (A6b), and (A6c) become the following:

$$\left\{cc_l^e\right\}^s = \left(\left[A^s\right] - q[E]\right)^{-1}\left(q[E]\left[A^s\right]^{-1}\{1\}\alpha^r + q[F]\{c_m\} - [G]\{m_w g\}\right) \tag{A8a}$$

$$\left\{cc_l^e\right\}^a = \left(\left[A^a\right] - q[E]\right)^{-1}\left(q[E]\left\{cc_l^r\right\}_{\delta_a}^a\ \delta_a + q[F]\{c_m\}_{\delta_a}\ \delta_a\right) \tag{A8b}$$

$$\left\{cc_l^e\right\}^{as} = \left(\left[A^{as}\right] - q[E]\right)^{-1}\left(q[E]\left[A^{as}\right]^{-1}\{\alpha\}_{FF}\right) \tag{A8c}$$

Finally, apply the relationship $\left\{cc_l^e\right\} = [A]^{-1}\{\theta\}$ to get equations (17a), (17b), and (17c).

$$\{\theta\}^s = \left[A^s\right]\left(\left[A^s\right] - q[E]\right)^{-1}\left(q[E]\{1\}\alpha^r + q[F]\{c_m\} - [G]\left\{\tfrac{1}{2}m_w g\right\}\right) \tag{17a}$$

$$\{\theta\}^a = \left[A^a\right]\left(\left[A^a\right] - q[E]\right)^{-1}\left(q[E]\left\{cc_l^r\right\}_{\delta_a}^a \delta_a + q[F]\{c_m\}_{\delta_a}\delta_a\right) \tag{17b}$$

$$\{\theta\}^{as} = \left[A^{as}\right]\left(\left[A^{as}\right] - q[E]\right)^{-1}\left(q[E]\left[A^{as}\right]^{-1}\{\alpha\}_{FF}\right) \tag{17c}$$

APPENDIX B
DERIVATION OF EQUATION 19

The torsional influence function can be computed for each wing from equation 2-120 of Bisplinghoff (ref. 11):

$$C^{\theta\theta} = \int_0^{b/2} \frac{dy}{GJ} \tag{B1}$$

In order to evaluate the torsional influence function integral equation (B1) directly, the torsional rigidity GJ must be written in terms of the span-wise coordinate y. For a single cell box, the torsional rigidity is computed from equation 2-125 of Bisplinghoff (ref. 11):

$$GJ = G\frac{4A^2}{\oint \frac{ds}{t}} \tag{B2}$$

From the wing box geometry shown in figure 4, the dimensions of the wing box are:

$$\begin{aligned} \text{length} &= \frac{1}{2}c \\ \text{height} &= \gamma\, c \end{aligned} \tag{B3}$$

Under the assumption that the material thickness is constant, the integral in the denominator of equation (B2) for a rectangular wing box is simply the perimeter divided by the material thickness as shown in equation (B4):

$$\oint \frac{ds}{t} = \frac{1}{t}\left[2\left(\gamma c + \tfrac{1}{2}c\right)\right] \tag{B4}$$

The area of the wing box is easily found as:

$$A = (\gamma c)\left(\tfrac{1}{2}c\right) \tag{B5}$$

The rigidity equation can now be written in terms of chord length by substituting equations (B4) and (B5) into equation (B2):

$$GJ = \frac{4tG\left[(\gamma c)\left(\frac{1}{2}c\right)\right]^2}{2\left(\gamma c + \frac{1}{2}c\right)} \quad \rightarrow \quad GJ = \frac{tG\gamma^2}{2\gamma + 1}c^3 \tag{B6}$$

Chord length is related to the span-wise coordinate y through the taper ratio. The example sailplane has a two-piece wing with different taper ratios for the inner and outer sections. Let $y(\Delta\lambda)$ indicate the point along the wing where the taper ratio changes and c_r be the chord length at the wing root. The inner and outer taper ratios are then defined as follows:

$$\lambda_i \equiv \left.\frac{c(y)}{c_r}\right|_{y=\Delta\lambda}, \text{ and } \lambda_o \equiv \left.\frac{c(y)}{c_r}\right|_{y=\frac{1}{2}b} \tag{B7}$$

The chord length of each wing section varies linearly with the span, according to equation (B8):

$$\begin{aligned} c(y)_i &= \left(\frac{dc}{dy}\right)_i y + a_i \quad , \quad y \le y(\Delta y) \\ c(y)_o &= \left(\frac{dc}{dy}\right)_i y + a_o \quad , \quad y > y(\Delta y) \end{aligned} \tag{B8}$$

Evaluating the slope and intercept for the inner section:

$$\left(\frac{dc}{dy}\right)_i = \frac{c(y)\big|_{y=0} - c(y)\big|_{y=y(\Delta\lambda)}}{0 - y(\Delta\lambda)} = -\frac{c_r - c_r\lambda_i}{y(\Delta\lambda)} \tag{B9}$$

$$a_i = c(y)\big|_{y=0} \quad \rightarrow \quad a_i = c_r \tag{B10}$$

The chord length for the inner wing half, then, is:

$$c(y)_i = c_r\left[1 - \left(\frac{1-\lambda_i}{y(\Delta\lambda)}\right)y\right] \quad , \quad 0 \le y \le y(\Delta\lambda) \tag{B11}$$

The outer wing half equation is similarly developed by evaluating equation (B-8) at the $y(\Delta\lambda)$ station and at the wing tip, $y = \frac{1}{2}b$:

$$\begin{aligned} c(y)_o\big|_{y=y(\Delta y)} &= \left(\frac{dc}{dy}\right)_o y(\Delta\lambda) + a_o = c_r\lambda_i \\ c(y)_o\big|_{y=\frac{1}{2}b} &= \left(\frac{dc}{dy}\right)_o \left(\tfrac{1}{2}b\right) + a_o = c_r\lambda_o \end{aligned} \tag{B12}$$

Solving these two equations simultaneously yields:

$$\left(\frac{dc}{dy}\right)_o = \frac{c_r(\lambda_i - \lambda_o)}{y(\Delta\lambda) - \frac{1}{2}b}, \text{ and } a_o = c_r \frac{\frac{1}{2}b\lambda_i - \lambda_o y(\Delta\lambda)}{\frac{1}{2}b - y(\Delta\lambda)} \tag{B13}$$

The chord length of the outer wing half, then, is:

$$c(y)_o = c_r\left[\left(\frac{\frac{1}{2}b\lambda_i - \lambda_o y(\Delta\lambda)}{\frac{1}{2}b - y(\Delta\lambda)}\right) - \left(\frac{\lambda_i - \lambda_o}{\frac{1}{2}b - y(\Delta\lambda)}\right)y\right], \qquad y(\Delta\lambda) \le y \le \tfrac{1}{2}b \tag{B14}$$

The constants are defined:

$$k \equiv \frac{tG\gamma^2 c_r^3}{2\gamma^2 + 1} \tag{B15a}$$

$$k_i \equiv \frac{1 - \lambda_i}{y(\Delta\lambda)} \tag{B15b}$$

$$k_o^1 \equiv \frac{\frac{1}{2}b\lambda_i - \lambda_o y(\Delta\lambda)}{\frac{1}{2}b - y(\Delta\lambda)} \tag{B15c}$$

$$k_o^2 \equiv \frac{\lambda_i - \lambda_o}{\frac{1}{2}b - y(\Delta\lambda)} \tag{B15d}$$

Equations (B11) and (B14) are then written as:

$$c(y)=\begin{cases} c_r\left[1-k_i y\right] \quad , & 0\le y\le y(\Delta\lambda) \\ c_r\left[k_o^1-k_o^2 y\right], & y(\Delta\lambda)\le y\le \frac{1}{2}b \end{cases} \tag{B16}$$

Substituting equations (B6) and (B16) into equation (B1) and integrating piecewise over the inner and outer wing sections gives the torsional influence function $C^{\theta\theta}$. The inner section integral is evaluated as:

$$C_i^{\theta\theta}=\int_0^y \frac{dy}{GJ}=\int_0^y \frac{dy}{\frac{tG\gamma^2}{2\gamma+1}c_i^3}=\int_0^y \frac{dy}{\left[\frac{tG\gamma^2}{2\gamma+1}\right]\left[c_r\left(1-k_i y\right)\right]^3}=\frac{1}{k}\int_0^y \left(1-k_i y\right)^{-3}dy$$

let

$$u=1-k_i y$$
$$du=-k_i dy$$

then

$$C_i^{\theta\theta}=\frac{-1}{kk_i}\int_0^y u^{-3}\,du \quad\rightarrow\quad C_i^{\theta\theta}=\frac{-1}{kk_i}\left[\frac{u^{-2}}{-2}\right]_0^y \quad\rightarrow\quad C_i^{\theta\theta}=\frac{1}{2kk_i}\left[\left(1-k_i y\right)^{-2}-1\right] \tag{B17}$$

The outer section integral is evaluated similarly:

$$C_o^{\theta\theta} = \int_{y(\Delta\lambda)}^{y} \frac{dy}{\frac{tG\gamma^2}{2\gamma+1}c_o^3} = \int_{y(\Delta\lambda)}^{y} \frac{dy}{\left[\frac{tG\gamma^2}{2\gamma+1}\right]\left[c_r\left(k_o^1 - k_o^2 y\right)\right]^3} = \frac{1}{k}\int_{y(\Delta\lambda)}^{y} \left(k_o^1 - k_o^2 y\right)^{-3} dy$$

let

$$C_o^{\theta\theta} = \int_{y(\Delta\lambda)}^{y} \frac{dy}{\frac{tG\gamma^2}{2\gamma+1}c_o^3} = \int_{y(\Delta\lambda)}^{y} \frac{dy}{\left[\frac{tG\gamma^2}{2\gamma+1}\right]\left[c_r\left(k_o^1 - k_o^2 y\right)\right]^3} = \frac{1}{k}\int_{y(\Delta\lambda)}^{y} \left(k_o^1 - k_o^2 y\right)^{-3} dy$$

let

$$u = k_o^1 - k_o^2 y$$
$$du = -k_o^2 dy$$

then

$$C_o^{\theta\theta} = \frac{-1}{kk_o^2}\int_{y(\Delta\lambda)}^{y} u^{-3}\, du \quad \rightarrow \quad C_o^{\theta\theta} = \frac{-1}{kk_o^2}\left[\frac{u^{-2}}{-2}\right]_{y(\Delta\lambda)}^{y} \quad \rightarrow$$
$$C_o^{\theta\theta} = \frac{1}{2kk_o^2}\left[\left(k_o^1 - k_o^2 y\right)^{-2} - \left(k_o^1 - k_o^2 y(\Delta\lambda)\right)^{-2}\right] \tag{B18}$$

Equation (19), the piecewise expression for the torsional influence function, follows from equations (B17) and (B18):

$$C^{\theta\theta} = \frac{1}{2kk_i}\left[\frac{1}{(1-k_i y)^2} - 1\right], \qquad 0 \le y \le y(\Delta\lambda)$$
$$C^{\theta\theta} = C^{\theta\theta}\left(y(\Delta\lambda)\right) + \frac{1}{2kk_o^2}\left[\frac{1}{\left(k_o^1 - k_o^2 y\right)^2} - \frac{1}{\left(k_o^1 - k_o^2 y(\Delta\lambda)\right)^2}\right], \qquad y(\Delta\lambda) \le y \le \tfrac{1}{2}b \tag{B19}$$

REPORT DOCUMENTATION PAGE

Form Approved
OMB No. 0704-0188

1. REPORT DATE *(DD-MM-YYYY)*	2. REPORT TYPE	3. DATES COVERED *(From - To)*
01-08-2009	Technical Memorandum	

4. TITLE AND SUBTITLE
Static Aeroelastic Effects of Formation Flight for Slender Unswept Wings

5a. CONTRACT NUMBER

5b. GRANT NUMBER

5c. PROGRAM ELEMENT NUMBER

6. AUTHOR(S)
Curtis E. Hanson

5d. PROJECT NUMBER

5e. TASK NUMBER

5f. WORK UNIT NUMBER

7. PERFORMING ORGANIZATION NAME(S) AND ADDRESS(ES)
NASA Dryden Flight Research Center
P.O. Box 273
Edwards, California 93523-0273

8. PERFORMING ORGANIZATION REPORT NUMBER
H-2980

9. SPONSORING/MONITORING AGENCY NAME(S) AND ADDRESS(ES)
National Aeronautics and Space Administration
Washington, DC 20546-001

10. SPONSORING/MONITOR'S ACRONYM(S)
NASA

11. SPONSORING/MONITORING REPORT NUMBER
NASA/TM-2009-214649

12. DISTRIBUTION/AVAILABILITY STATEMENT
Unclassified -- Unlimited
Subject Category 02, 05, 39 Availability: NASA CASI (301) 621-0390 Distribution: Standard

13. SUPPLEMENTARY NOTES
Hanson, NASA Dryden Flight Research Center.

14. ABSTRACT

The static aeroelastic equilibrium equations for slender, straight wings are modified to incorporate the effects of aerodynamically-coupled formation flight. A system of equations is developed by applying trim constraints and is solved for component lift distribution, trim angle-of-attack, and trim aileron deflection. The trim values are then used to calculate the elastic twist distribution of the wing box. This system of equations is applied to a formation of two gliders in trimmed flight. Structural and aerodynamic properties are assumed for the gliders, and solutions are calculated for flexible and rigid wings in solo and formation flight. It is shown for a sample application of two gliders in formation flight, that formation disturbances produce greater twist in the wingtip immersed in the vortex than for either the opposing wingtip or the wings of a similar airplane in solo flight. Changes in the lift distribution, resulting from wing twist, increase the performance benefits of formation flight. A flexible wing in formation flight will require greater aileron deflection to achieve roll trim than a rigid wing.

15. SUBJECT TERMS
Aeroelastic wing twist, Drag reduction, Formation flight, Sailplane, Wingtip vortices

16. SECURITY CLASSIFICATION OF:			17. LIMITATION OF ABSTRACT	18. NUMBER OF PAGES	19b. NAME OF RESPONSIBLE PERSON
a. REPORT	b. ABSTRACT	c. THIS PAGE			STI Help Desk (443) 757-5802
					19b. TELEPHONE NUMBER *(Include area code)*
U	U	U	UU	35	(443) 757-5802